Large-mode enhancement cavities

Henning Carstens,[1,2] **Simon Holzberger,**[1,2] **Jan Kaster,**[1,2]
Johannes Weitenberg,[3] **Volodymyr Pervak,**[2] **Alexander Apolonski,**[1,2]
Ernst Fill,[1,2] **Ferenc Krausz,**[1,2] **and Ioachim Pupeza**[1,2,*]

[1] *Max-Planck-Institut für Quantenoptik, Hans-Kopfermann-Str. 1, 85748 Garching, Germany*
[2] *Ludwig-Maximilians-Universität München, Department für Physik, Am Coulombwall 1, 85748 Garching, Germany*
[3] *RWTH Aachen University, Lehrstuhl für Lasertechnik, Steinbachstr. 15, 52074 Aachen, Germany*
[*] *ioachim.pupeza@mpq.mpg.de*

Abstract: In passive enhancement cavities the achievable power level is limited by mirror damage. Here, we address the design of robust optical resonators with large spot sizes on all mirrors, a measure that promises to mitigate this limitation by decreasing both the intensity and the thermal gradient on the mirror surfaces. We introduce a misalignment sensitivity metric to evaluate the robustness of resonator designs. We identify the standard bow-tie resonator operated close to the inner stability edge as the most robust large-mode cavity and implement this cavity with two spherical mirrors with 600 mm radius of curvature, two plane mirrors and a roundtrip length of 1.2 m, demonstrating a stable power enhancement of near-infrared laser light by a factor of 2000. Beam radii of 5.7 mm $\times$ 2.6 mm (sagittal $\times$ tangential $1/e^2$ intensity radius) on all mirrors are obtained. We propose a simple all-reflective ellipticity compensation scheme. This will enable a significant increase of the attainable power and intensity levels in enhancement cavities.

OCIS codes: (140.4780) Optical resonators; (140.7240) UV, EUV, and X-ray lasers.

References and links

1. A. Ashkin, G. Boyd, and J. Dziedzic, "Resonant optical second harmonic generation and mixing," IEEE J. Quant. Electron. **2**, 109–124 (1966).
2. I. Pupeza, *Power Scaling of Enhancement Cavities for Nonlinear Optics* (Springer, 2012).
3. A. Cingöz, D. C. Yost, T. K. Allison, A. Ruehl, M. E. Fermann, I. Hartl, and J. Ye, "Direct frequency comb spectroscopy in the extreme ultraviolet," Nature **482**, 68–71 (2012).
4. I. Pupeza, T. Eidam, J. Rauschenberger, B. Bernhardt, A. Ozawa, E. Fill, A. Apolonski, T. Udem, J. Limpert, Z. A. Alahmed, A. M. Azzeer, A. Tünnermann, T. W. Hänsch, and F. Krausz, "Power scaling of a high-repetition-rate enhancement cavity," Opt. Lett. **35**, 2052–2054 (2010).
5. J. Lee, D. R. Carlson, and R. J. Jones, "Optimizing intracavity high harmonic generation for XUV fs frequency combs," Opt. Express **19**, 23315–23326 (2011).
6. C. Gohle, T. Udem, M. Herrmann, J. Rauschenberger, R. Holzwarth, H. A. Schuessler, F. Krausz, and T. W. Hänsch, "A frequency comb in the extreme ultraviolet," Nature **436**, 234–237 (2005).
7. R. J. Jones, K. D. Moll, M. J. Thorpe, and J. Ye, "Phase-coherent frequency combs in the vacuum ultraviolet via high-harmonic generation inside a femtosecond enhancement cavity," Phys. Rev. Lett. **94**, 193201 (2005).
8. T. K. Allison, A. Cingöz, D. C. Yost, and J. Ye, "Extreme nonlinear optics in a femtosecond enhancement cavity," Phys. Rev. Lett. **107**, 183903 (2011).
9. D. R. Carlson, J. Lee, J. Mongelli, E. M. Wright, and R. J. Jones, "Intracavity ionization and pulse formation in femtosecond enhancement cavities," Opt. Lett. **36**, 2991–2993 (2011).

#188266 - $15.00 USD Received 3 Apr 2013; revised 23 Apr 2013; accepted 27 Apr 2013; published 3 May 2013

10. I. Pupeza, S. Holzberger, T. Eidam, H. Carstens, D. Esser, J. Weitenberg, P. Rußbüldt, J. Rauschenberger, J. Limpert, T. Udem, A. Tünnermann, T. Hänsch, A. Apolonski, F. Krausz, and E. Fill, "Compact high-repetition-rate source of coherent 100-electronvolt radiation," accepted for publication in Nat. Photonics (2013).
11. I. B. Angelov, A. v. Conta, S. A. Trushin, Z. Major, S. Karsch, F. Krausz, and V. Pervak, "Investigation of the laser-induced damage of dispersive coatings," Proc. SPIE **8190**, 81900B (2011).
12. M. Mero, J. Liu, W. Rudolph, D. Ristau, and K. Starke, "Scaling laws of femtosecond laser pulse induced breakdown in oxide films," Phys. Rev. B **71** (2005).
13. M. Theuer, D. Molter, K. Maki, C. Otani, J. A. L'huillier, and R. Beigang, "Terahertz generation in an actively controlled femtosecond enhancement cavity," Appl. Phys. Lett. **93**, 041119–3 (2008).
14. K. Sakaue, M. Washio, S. Araki, M. Fukuda, Y. Higashi, Y. Honda, T. Omori, T. Taniguchi, N. Terunuma, J. Urakawa, and N. Sasao, "Observation of pulsed x-ray trains produced by laser-electron Compton scatterings," Rev. Sci. Instrum. **80**, 123304–123304–7 (2009).
15. A. Gerrard and J. M. Burch, *Introduction to Matrix Methods in Optics* (Wiley, 1975).
16. H. Kogelnik and T. Li, "Laser beams and resonators," Proc. IEEE **54**, 1312–1329 (1966).
17. V. Magni, "Multielement stable resonators containing a variable lens," J. Opt. Soc. Am. A **4**, 1962–1969 (1987).
18. S. d. Silvestri, P. Laporta, and V. Magni, "Rod thermal lensing effects in solid-state laser ring resonators," Opt. Commun. **65**, 373–376 (1988).
19. S. Gigan, L. Lopez, N. Treps, A. Maître, and C. Fabre, "Image transmission through a stable paraxial cavity," Phys. Rev. A **72**, 023804 (2005).
20. N. Hodgson and H. Weber, "Misalignment sensitivity of stable resonators in multimode operation," J. Mod. Opt. **39**, 1873–1882 (1992).
21. R. Hauck, H. P. Kortz, and H. Weber, "Misalignment sensitivity of optical resonators," Appl. Opt. **19**, 598–601 (1980).
22. W. B. Joyce and B. C. DeLoach, "Alignment of Gaussian beams," Appl. Opt. **23**, 4187–4196 (1984).
23. F. Kawazoe, R. Schilling, and H. Lück, "Eigenmode changes in a misaligned triangular optical cavity," J. Opt. **13**, 055504 (2011).
24. A. Fox and T. Li, "Resonant modes in a maser interferometer," Bell Syst. Tech. J **40**, 453–488 (1961).
25. E. Constant, D. Garzella, P. Breger, E. Mével, C. Dorrer, C. Le Blanc, F. Salin, and P. Agostini, "Optimizing high harmonic generation in absorbing gases: model and experiment," Phys. Rev. Lett. **82**, 1668–1671 (1999).
26. C. M. Heyl, J. Güdde, A. L'Huillier, and U. Höfer, "High-order harmonic generation with μJ laser pulses at high repetition rates," J. Phys. B **45**, 074020 (2012).
27. A. Ozawa, A. Vernaleken, W. Schneider, I. Gotlibovych, T. Udem, and T. W. Hänsch, "Non-collinear high harmonic generation: a promising outcoupling method for cavity-assisted XUV generation," Opt. Express **16**, 6233–6239 (2008).
28. K. D. Moll, R. J. Jones, and J. Ye, "Output coupling methods for cavity-based high-harmonic generation," Opt. Express **14**, 8189–8197 (2006).
29. T. Heupel, M. Weitz, and T. W. Hänsch, "Phase-coherent light pulses for atom optics and interferometry," Opt. Lett. **22**, 1719 (1997).
30. G. Mourou, B. Brocklesby, T. Tajima, and J. Limpert, "The future is fibre accelerators," Nat. Photonics **7**, 258–261 (2013).
31. J. Weitenberg, P. Rußbüldt, T. Eidam, and I. Pupeza, "Transverse mode tailoring in a quasi-imaging high-finesse femtosecond enhancement cavity," Opt. Express **19**, 9551–9561 (2011).
32. W. P. Putnam, D. N. Schimpf, G. Abram, and F. X. Kärtner, "Bessel-Gauss beam enhancement cavities for high-intensity applications," Opt. Express **20**, 24429–24443 (2012).
33. J. A. Arnaud, "Degenerate optical cavities," Appl. Opt. **8**, 189–195 (1969).
34. T. J. Kane and R. L. Byer, "Monolithic, unidirectional single-mode Nd:YAG ring laser," Opt. Lett. **10**, 65–67 (1985).
35. R. W. P. Drever, J. L. Hall, F. V. Kowalski, J. Hough, G. M. Ford, A. J. Munley, and H. Ward, "Laser phase and frequency stabilization using an optical resonator," Appl. Phys. B **31**, 97–105 (1983).
36. H. Kogelnik, E. Ippen, A. Dienes, and C. Shank, "Astigmatically compensated cavities for CW dye lasers," IEEE J. Quant. Electron. **8**, 373–379 (1972).
37. D. Sigg and N. Mavalvala, "Principles of calculating the dynamical response of misaligned complex resonant optical interferometers," J. Opt. Soc. Am. A **17**, 1642–1649 (2000).
38. F. Zomer, Y. Fedala, N. Pavloff, V. Soskov, and A. Variola, "Polarization induced instabilities in external four-mirror Fabry-Perot cavities," Appl. Opt. **48**, 6651–6661 (2009).

#188266 - $15.00 USD Received 3 Apr 2013; revised 23 Apr 2013; accepted 27 Apr 2013; published 3 May 2013

1. Introduction

Passive optical resonators can be efficiently excited by light emitted from a single-frequency or modelocked laser as its coherence allows for a constant phase relationship of the incident field with the field inside the resonator. Under proper resonance conditions, energy is continuously coupled to the *enhancement cavity* (EC) and the power circulating in the cavity can be several orders of magnitude larger than the input power. The enhancement is limited by the resonator round trip losses and, in the case of pulsed light, by chromatic dispersion. In general the efficiency of optical frequency conversion processes increases with the driving intensity and thus the EC technique lends itself to the efficient conversion of laser light to short wavelengths in the extreme-ultraviolet (XUV) or the THz spectral region.

Shortly after the invention of the laser, the potential of ECs was demonstrated for the efficient conversion of continuous-wave radiation to its second harmonic [1]. Numerous further applications and a wide range of variations of this technique followed, including its extension to the operation with ultrashort pulses (an overview is given in Section 1.2 of Ref. [2]). The resonant enhancement of pulsed radiation is made possible by the comb-like structure of the spectrum emitted by a modelocked laser which allows coupling each individual comb line to a cavity resonance. In the time domain this means that the cavity round trip time is equal to a multiple of the pulse repetition period. This makes ECs suitable for the enhancement of pulse trains with repetition rates between $\sim$10 MHz and several GHz. Recently, average powers on the order of a few kW [3–5] have been reached with near-infrared intracavity femtosecond pulses around 100 MHz with peak intensities exceeding 10^{14} W/cm^2. Higher power and intensity levels are, however, impeded by intensity-related mirror damages. For a 80 MHz enhancement-cavity with 200 fs pulses the maximum obtainable average power was determined to be 18 kW [4].

One of the main motivations for the development of femtosecond ECs has been the generation of XUV radiation via high-order harmonic generation (HHG) [6, 7]. Here, the achievable intensity levels are currently limited by ionization-related effects in the gas target [8, 9]. Recently it has been shown that these effects can be efficiently mitigated by decreasing the duration of the enhanced pulses [10]. A possible approach to designing highly reflecting mirrors supporting the necessary bandwidth is employing materials with low band gaps (and thus high refractive indices). However, this comes at the expense of a damage threshold which is significantly lower than for high-band-gap materials [11]. Furthermore, the damage threshold fluence decreases for a given material with the pulse duration [12]. To overcome the limitation of mirror damage and enable a further scaling of the attainable power and intensity levels in these systems, increasing the spot sizes on all mirrors is mandatory. The same strategy promises to benefit other EC-assisted conversion processes, such as THz generation [13] or Thomson (inverse Compton) scattering experiments, where typically picoseconds pulses are used [14]. For the latter, the number of generated X-ray photons increases linearly with the laser power.

The scope of this article is to investigate theoretically and experimentally the robustness of different approaches for obtaining large beam sizes on the cavity mirrors. Based on the well-known matrix formalism for the description of resonators, a new misalignment sensitivity metric specifically for enhancement cavities is introduced in Section 2. Based on this, different resonator designs with large beam sizes on all cavity optics are compared in Section 3. In Section 4 the experimental implementation of these designs is presented and the standard bow tie resonator, consisting of two spherical and two plane mirrors is identified as the most robust large-mode ring resonator. In Section 5 we discuss all-reflective schemes for astigmatism compensation. Section 6 concludes the paper.

#188266 - $15.00 USD Received 3 Apr 2013; revised 23 Apr 2013; accepted 27 Apr 2013; published 3 May 2013

2. Theoretical models

2.1. Misaligned stable resonators

In this paper we use the 3×3 matrix formalism [15] for the analysis of planar passive resonators, which extends the well-known ABCD-matrix formalism [16] by misaligned optical elements. A system matrix M, describing a round trip through the (misaligned) resonator, can be obtained by matrix multiplication of the individual elements. The system matrix M reads:

$$M = \begin{pmatrix} A & B & \Delta x \\ C & D & \Delta\alpha \\ 0 & 0 & 1 \end{pmatrix}. \tag{1}$$

The upper left 2×2 sub-matrix is the conventional ABCD matrix and thus allows for the calculation of the eigenmode if the cavity is stable, i.e. if $-2 < A+D < 2$ holds [16]. The misalignment is described by the matrix elements Δx and $\Delta\alpha$. For the system matrix M, these quantities can be interpreted as the offset and angle, respectively, of the optical axis of the unperturbed resonator $(0,0,1)^{\mathrm{T}}$ after one round trip through the resonator. Corresponding values for optical elements such as lenses or mirrors can be found e.g. in [17]. We consider only the fundamental Gaussian mode, but the extension to higher-order modes is straightforward. Note that this sub-matrix is independent of any misalignment in the frame of the 3×3-matrix-formalism, i.e. the eigenmode is not affected. This approximation holds only for small misalignments, e.g. for small mirror tilts that do not significantly change distances between two elements.

At the stability edge, the eigenmode exhibits a divergent behavior, i.e. large spot sizes can be obtained. Any misalignment of elements causes a change of the optical axis, defined as the ray that reproduces itself after one roundtrip through the resonator. It can be calculated from the elements of the system matrix M as [15]

$$x_0 = \frac{(1-D)\Delta x + B\Delta\alpha}{2-A-D}, \tag{2}$$

$$V_0 = \frac{(1-A)\Delta\alpha + C\Delta x}{2-A-D}. \tag{3}$$

Here, x_0 and V_0 denote the offset and the angle of the new optical axis, respectively, in a reference plane with respect to that of the unperturbed resonator. The displacement of the optical axis diverges in general for $A+D=+2$, i.e. at one of the stability edges, but not for the other edge ($A+D=-2$). In [18], Silvestri et al. found, that the sensitivity for rod thermal lensing in a ring resonator is minimized at this edge.

The stability can also be interpreted in terms of the Gouy phase. The accumulated Gouy phase ϕ_{Gouy} of the fundamental mode for one round-trip through a stable resonator is given by [19]

$$\phi_{\mathrm{Gouy}} = \arccos\left(\frac{A+D}{2}\right). \tag{4}$$

At the stability edge with diverging alignment sensitivity ($A+D=+2$), the Gouy-phase is $0+2\pi N$, and at the other edge $\pi+2\pi N$, where N is an integer. The accumulated Gouy phase shift upon propagation through a focus (propagation distance much larger than the Rayleigh length) is π. Therefore, if we can subdivide a resonator into N strongly focused arms (corresponding to $\phi_{\mathrm{Gouy}} \approx \pi$ in each arm) and collimated arms (corresponding to $\phi_{\mathrm{Gouy}} \approx 0$) – as it is typical for resonators at a stability edge – the total Gouy-phase is $N\pi$. In conclusion, for even numbers of strongly focused arms, the alignment sensitivity diverges, while for odd numbers the resonator is robust with respect to misalignment.

#188266 - $15.00 USD Received 3 Apr 2013; revised 23 Apr 2013; accepted 27 Apr 2013; published 3 May 2013

2.2. Quantification of the alignment sensitivity for enhancement cavities

The effect of misalignment on the operation of a resonator depends on the application. In case of lasers, i.e. resonators containing an active medium, metrics for the alignment sensitivity based on the output power variation due to the overlap of the eigenmode with the pumped volume in the active medium [20] and the variation of diffraction losses at finite apertures in the cavity due to misalignment [21] are used. For enhancement cavities the physical situation is different: light from an external source is coupled to the resonator and the coupling efficiency depends on the spatial overlap between the incoming beam and the circulating field. Any perturbation of the resonator alignment – either of the q-parameter, or in orientation of the optical axis – also changes the overlap of the two beams. The change in overlap therefore is a physically meaningful metric for the alignment sensitivity of enhancement cavities. As the overlap integral is a conserved quantity upon propagation through lens-like media, it can be evaluated anywhere in the cavity, although the interference between the two beams physically takes place at the input coupler. This is a strong feature of this metric, as any perturbation can be mapped to a single number (the change in overlap) that does not depend on a reference plane in the cavity. The overlap can be calculated between the eigenmode $\Psi_{\text{initial}}(x,y)$ before and $\Psi_{\text{pert}}(x,y)$ after a perturbation. Mathematically, it is given by the overlap integral [22]:

$$U = \left| \int_{-\infty}^{\infty} \Psi_{\text{initial}}(x,y)\Psi^*_{\text{pert}}(x,y)\mathrm{d}x\mathrm{d}y \right|^2 , \tag{5}$$

where $\Psi_{\text{inital}}(x,y)$ and $\Psi_{\text{pert}}(x,y)$ are the normalized complex transverse field distributions.

We will use the 3×3-matrix-formalism described above for calculating the initial and perturbed eigenmodes. Note that alternatively ray-tracing, geometrical analysis [23] or numerical algorithms such as Fox-Li [24] can be used to evaluate U, in case the cavity or the perturbations cannot be described by 3×3-matrices. The 3×3-matrix-formalism describes two fundamental types of perturbations. Longitudinal perturbations (described by the conventional ABCD formalism) only change the eigenmode and transverse perturbations (described by the misalignment parameters in the 3×3 matrix) only change the orientation of the optical axis. Examples for the former are lengths changes and thermal lenses and for the latter mirror tilts and lens offsets. For transverse perturbations, the eigenmode with an offset x_0 and a (small) tilt V_0 (both in x direction), but equal transverse field distribution, can be written as [22]

$$\Psi_{\text{pert}}(x,y) = \Psi_{\text{inital}}(x-x_0,y)e^{ikV_0x}, \tag{6}$$

with the wavenumber $k = 2\pi/\lambda$.

3. Cavity designs

3.1. Design considerations

Due to the fundamental requirement of a large resonator finesse, only optically stable resonators are considered here. In the center of the stability range, the maximum spot size is proportional to the cavity length. The achievable power inside the enhancement cavity is limited by the damage threshold of the optics given by some fluence $F = P/(c\lambda)$ (optical power P, speed of light c and wavelength λ), this limits. Larger spot sizes on the mirrors and therefore a higher power can only be obtained at a stability edge or in a longer cavity. As the cavity round-trip time must be an integer multiple of the pulse repetition period, the length can be increased even for a fixed repetition rate of the seeding laser, however at the expense of a narrower cavity resonance linewidth. Therefore, operating the EC at a stability edge can be a more robust approach. To

#188266 - $15.00 USD Received 3 Apr 2013; revised 23 Apr 2013; accepted 27 Apr 2013; published 3 May 2013

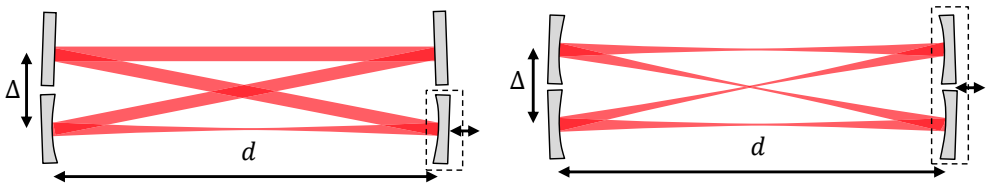

(a) Standard bow-tie (SBT) cavity (b) All-curved-mirror (ACM) cavity

Fig. 1. (a) Standard bow-tie (SBT) cavity consisting of two focusing mirrors and two plane mirrors, operated close to the inner stability edge. (b) All-curved-mirror (ACM) cavity with four equal focusing mirrors and two overlapping foci. The distance d denotes the geometric separation between opposite curved mirrors. For the ACM cavity, an increase of d also increases the cavity length, while for the SBT the distance d can be chosen in a certain range.

improve the ratio of the intensity at the focus to that on the subsequent mirror assuming a given focus size, weaker focusing mirrors with larger separation distance have to be used. This maximum separation is limited by the cavity length, so this ratio might impose a lower bound on the cavity length. Based on these considerations, we discuss cavity designs that allow for an increase on *all* optics in the cavity simultaneously. In particular for HHG, a larger focus is favorable, as the harmonic yield scales at least quadratically with the focus radius [25] and a longer Rayleigh length is often advantageous for phase-matching in a tight focus regime [26].

We investigate two ring resonator designs: The standard bow-tie (SBT) Cavity (one arm is strongly focused, the other is collimated) and the all-curved-mirror (ACM) resonator with four focused arms, both shown in Fig. 1. These two resonators share the following features:

- The angles of incidence on the mirrors are small, which implies only weak astigmatism when using spherical optics.
- Due to the symmetry with respect to the focal planes, the beam waist is always centered between the curved mirrors for both the sagittal and the tangential plane, such that the small astigmatism introduced by the non-zero angle of incidence on the spherical mirrors manifests itself as a pure ellipticity of the eigenmode.
- The cavities are planar, so there is no geometric polarization rotation. If the difference in reflectivity for s- and p-polarized light can be neglected (as for small angles of incidence), any incoming polarization is preserved.
- For a given focus size, the diffraction limited fundamental Gaussian mode considered here exhibits the largest possible focal volume (i.e. the volume, where the intensity is larger than some threshold).

Further designs, that do not exhibit all of these features, are discussed in Section 3.4.

3.2. The standard bow-tie cavity

The SBT of length L consists of two identical spherical mirrors (radius of curvature R) separated by a distance d and some folding mirrors as shown in Fig. 1(a). The distance d between the focusing mirrors can be increased up to $L/2$ for a triangular three-mirror cavity. Provided that $R \leq L/4$ holds, the SBT is stable for $R < d < L/2 - \sqrt{L^2 - 4RL}/2$. For $R > L/4$ the outer stability edge does not exist, so the cavity is stable up to the maximum possible distance $d = L/2$. For larger separations, the two distances d and $L - d$ are interchanged. Towards the inner

#188266 - $15.00 USD Received 3 Apr 2013; revised 23 Apr 2013; accepted 27 Apr 2013; published 3 May 2013

stability edge ($d = R$), the short arm is tightly focused and the long arm gets collimated, i.e. the spot size can be increased on all mirrors simultaneously. As discussed in Section 2.1, the alignment sensitivity does not diverge at this edge, because the round-trip Gouy phase is π. At the outer stability edge, both arms are focused (the Gouy-phase is 2π), so that the alignment sensitivity diverges and the spot size only grows on the curved mirrors, but not necessarily on the folding mirrors in between.

For a quantification of the transverse alignment sensitivity, we consider a $1\,\mu$rad tilt of one curved mirror in an astigmatism-free SBT and calculate the change in overlap over the entire stability zone (by variation of d) for a fixed cavity length and fixed radii of curvature of the focusing mirrors. When using typical kinematic 1" mirror mounts, this small tilt introduces a cavity length change of only about 50 nm. This effect of the misalignment on the absolute angle of incidence on the curved mirrors and on the cavity length is negligible for the range of parameters considered here. The result is shown in Fig. 2(a) where the beam size w_m ($1/e^2$-intensity radius) on the curved mirror indicates the position in the stability zone. Each cavity has a point of minimum sensitivity near, but not exactly at the smallest beam radius w_m. In general, this point is not the center of the stability zone. By approaching the outer stability edge (upper branch), the alignment sensitivity increases drastically, as the displacement of the optical axis diverges. In this branch, short cavities are more sensitive, as a given beam radius is obtained closer to the stability edge. Two SBT cavities of equal length, but with different focusing geometries, exhibit the same sensitivity towards the outer stability edge, as can be seen in the example of the 10 MHz cavities. By approaching the inner stability edge (lower branch), the sensitivity only increases moderately. Interestingly, the curves for all resonators converge towards the same inner edge, i.e. in this limit the alignment sensitivity depends only on the spot size on the mirrors, but not on the cavity geometry.

As the size of the eigenmode exhibits a divergent behavior at both stability edges, here the cavities are more susceptible to variations of the stability parameter. For a quantification of this longitudinal sensitivity, we calculate the overlap of the eigenmode before and after the distance d between two opposite curved mirrors (as defined in Fig. 1) is changed by some small value Δd, see Fig. 2(b). This leads again to two branches, the upper one being that of the inner stability edge. Equivalently, the overlap variation upon a change of the mirror curvature, as induced e.g. by thermal lensing, can be considered. For the example of the 125 MHz cavity, the longitudinal sensitivity increases by 7 orders of magnitude from the stability center to the point where the beam radius on the mirrors reaches 5 mm. This sensitivity will ultimately limit the achievable spot size. The longitudinal sensitivity decreases with increasing cavity length, as large spot sizes can be obtained closer to the stability center. Thus, increasing the cavity length offers a means to overcome limitations induced by the longitudinal sensitivity.

The above considered tilt of $1\,\mu$rad typically results in a cavity lenght change of only about 50 nm, a value much smaller than the considered longitudinal misalignment of $1\,\mu$m. Despite the smaller perturbation, the change in overlap is larger in the transverse case for the cavities shown in Fig. 2 at the inner stability edge. Therefore, the impact of mechanical vibrations with a certain amplitude will perturb this cavity mainly due to transverse effects, making the transverse alignment sensitivity the more important one. For the SBT the inner stability edge is expected to be more robust than the outer one, as here the transverse sensitivity is much lower. However, for perturbations that solely affect the cavity longitudinally (e.g. thermal lensing), the operation at the outer stability edge might be advantageous.

3.3. All-curved-mirror cavity

The all-curved-mirror (ACM) cavity depicted in Fig. 1(b) can be considered as a ring version of the concentric resonator. It consists of two adjacent pairs of identical curved mirrors separated

#188266 - $15.00 USD Received 3 Apr 2013; revised 23 Apr 2013; accepted 27 Apr 2013; published 3 May 2013

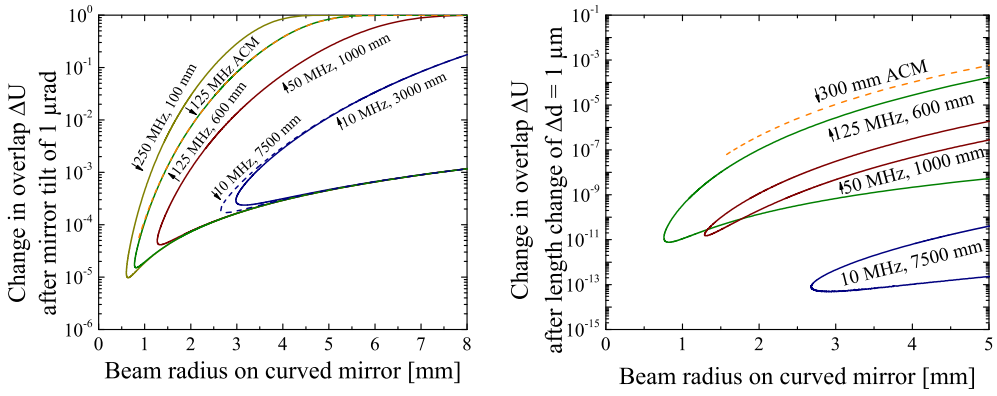

(a) Transverse sensitivity

(b) Longitudinal sensitivity

Fig. 2. The figures show the alignment sensitivity of several cavities by means of the change in overlap $\Delta U = 1 - U$ after a perturbation as a function of the beam radius on a curved mirror. (a) A curved mirror is tilted by an angle of $1\,\mu$rad, (b) The distance d is changed by $\Delta d = 1\,\mu$m.

by a distance d. For symmetry reasons, the spot sizes are the same on all mirrors. A particular feature of the ACM are the two crossing foci, which can be used e.g. for non-collinear HHG [27, 28]. The beam sizes can be increased on all mirrors simultaneously by increasing d towards the stability edge near $2R$, but here the number of strongly focused arms is even (round-trip Gouy phase approaches 4π), i.e. the alignment sensitivity diverges. There is no other stability edge with non-divergent alignment sensitivity for this resonator. Note that the double-bow-tie resonator suggested in [28] for non-collinear HHG also exhibits a diverging alignment sensitivity at the inner stability edge, as the round-trip Gouy phase is 2π.

The longitudinal and transverse sensitivity for a ACM cavity with radius of curvature 300 mm (repetition rate around 125 MHz) near the stability edge at $d = 2R$ are plotted in Fig. 2. The transverse sensitivity at this edge is the same as for the 125 MHz SBT cavity at its corresponding $A + D = +2$ edge, i.e. the more sensitive edge. The longitudinal sensitivity is slightly worse than that of an 125 MHz SBT at the inner stability edge. When large spot sizes on all cavity mirrors are desired, this design is disadvantageous in comparison with the SBT design in terms of robustness. However, it should be noted that the ACM cavity might be useful for applications where the effect on the position of the optical axis needs to be maximized for a given perturbation, such as output coupling for cavity-dumping [29, 30].

3.4. Alternative designs

In the following, we list alternative approaches that also enable a decrease of the intensity on the cavity optics, but do not satisfy at least on of the design criteria considered in this paper. However, the alignment sensitivity of these designs can be readily evaluated with the metric developed here.

- *Quasi-imaging* [31] *and Bessel-Gauss-beams* [32]: In these concepts, the circulating field can have an on-axis intensity maximum near the focus and avoids an on-axis opening in a mirror for output coupling of the frequency-converted light. As these beams are not diffraction-limited, the ratio of the intensity in (or close to) the focus to the intensity on a mirror is naturally higher for the same propagation distance. However, this is achieved at the cost of a reduced focal volume.

#188266 - $15.00 USD Received 3 Apr 2013; revised 23 Apr 2013; accepted 27 Apr 2013; published 3 May 2013

- *Imaging resonators* [33]: These are degenerate resonators, where arbitrary field distributions are reproduced after one round-trip. Large spot sizes on the mirrors could be obtained by coupling a large mode into the cavity.

- *Oblique incidence*: The illuminated area on a mirror can also be increased by choosing a large angle of incidence (AOI), as the area increases by a factor $1/\cos(\mathrm{AOI})$. This requires the use of toroidal or off-axis parabolic mirrors. Also, dielectric mirrors are in general polarization-discriminating for large AOI.

4. Experiments

4.1. Setup

We investigate two 125 MHz cavities, an ACM (R = 300 mm) operated close to $d = 2R$ and an SBT (R = 600 mm) operated close to $d = R$ in order to determine whether or not the operation close to the stability edge is constrained by the alignment sensitivity and/or mechanical vibrations in a laboratory environment. The cavities are tested in the setup shown in Fig. 3. We lock a single-frequency $\lambda = 1064$ nm non-planar ring oscillator (NPRO) [34] with the Pound-Drever-Hall locking scheme [35] to each cavity. Two photodiodes monitor the signal reflected by the input coupler. One is used to measure the power fraction coupled to the cavity K and the second one to obtain an error signal. The incoming beam is mode-matched to each cavity (round beam with spot size 3 mm at the respective input coupler) and is not changed throughout the experiments.

The enhancement factor E of the incoming power P_{in} is given by $P_{\mathrm{circ}}/P_{\mathrm{in}}$ where the circulating power P_{circ} can be measured via the transmission through a cavity mirror with known transmission. The cavity round trip power attenuation factor A that accounts for all losses except for those at the input coupler can be calculated according to $A = 1 - K/E$. The round trip power loss is given by $1 - A$. This analysis allows to distinguish between the overlap and the cavity losses (including diffraction losses at the mirror boundaries) as reasons for a change of the enhancement while the eigenmode is varied and the input field is kept constant. The intensity distribution at the surface of one of the mirrors is imaged to the CCD camera with known magnification (calibrated with an aperture of known size). From the measured beam size we determine the position in the stability zone. The beam ellipticity w_x/w_y provides an independent measurement, as the angles of incidence are known (1.24° for both cavities).

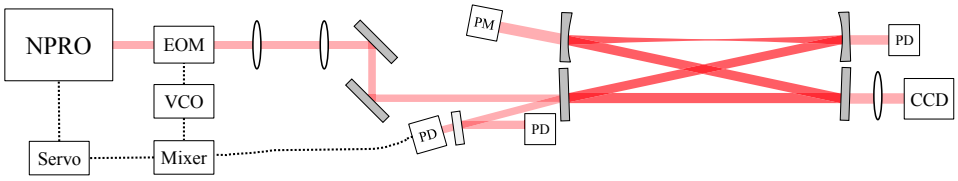

Fig. 3. Schematic of the experimental setup. NPRO: non-planar ring oscillator, EOM: electro-optical modulator, PD: photodiode, PM: power meter, CCD: CCD camera, VCO: voltage controlled oscillator.

4.2. Results

We locked the laser to each cavity at several positions in their stability zones and measured the beam size and the ellipticity on a cavity mirror. The results are shown in Fig. 4 together with theoretical curves calculated with the ABCD-matrix formalism. With the ACM cavity

#188266 - $15.00 USD Received 3 Apr 2013; revised 23 Apr 2013; accepted 27 Apr 2013; published 3 May 2013

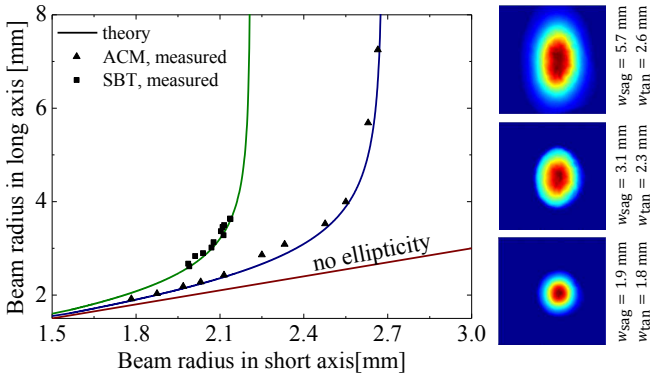

Fig. 4. Measured beam radii in both planes for the SBT and the ACM cavities while the stability edge was approached. The theoretical values are obtained with the ABCD-matrix formalism. For the SBT the long axis lies in the sagittal plane and for the ACM it lies in the tangential plane.

the maximum beam radii ($1/e^2$-intensity radius) in the two planes were 4 mm $\times$ 2.1 mm. At this position in the stability zone, the step size of 0.7 μrad of the motorized mirror mounts did not suffice for a satisfactory alignment. This confirms the behavior predicted by theory, as single steps already change the overlap by a few tens of percent. With the SBT cavity the alignment was significantly less critical. A spot size of 5.7 mm $\times$ 2.6 mm could be achieved without affecting the round trip attenuation. Even larger spots were obtained, however at the cost of diffraction losses at the mirror boundaries (25 mm in diameter). In principle this can be overcome by using larger mirrors. This, however, implies increased AOI, which further increases the ellipticity. Compared to the cavity described in Ref. [4], which can be considered as a benchmark for intensity-related power scaling limitations with a beam radius on the mirrors of 1 mm, a spot area increase by a factor of 8 and 15 was achieved with the ACM and the SBT cavity, respectively.

The RMS noise of the circulating power, transmitted through one of the cavity mirrors, was analyzed in the 20 Hz – 600 kHz band. The perturbations that might affect this signal are of two types: residual frequency noise of the laser relative to the cavity and variations of the overlap between the incoming beam and the eigenmode. Any increase in relative RMS noise towards the stability edge could therefore be attributed to the increased sensitivity of the cavity to mechanical perturbations. However, for both cavities, for all measurement points and for power enhancement factors ranging from 600 to 2000, the measured transmission signal RMS was independent on the position in the stability zone, remaining better than 0.1 % relative RMS.

In conclusion, we have identified the transverse alignment sensitivity as the limitation for an increase of spot size for the ACM cavity. For the SBT cavity, neither transverse, nor longitudinal alignment sensitivity constituted limitations, as expected from theory. Besides that, even at the stability edge no impact of the mechanical vibrations on the operation of the cavity could be detected with the above described measurement sensitivity.

5. Astigmatic compensation

5.1. In-plane compensation using astigmatic elements

Spherical mirrors irradiated under a non-zero AOI, introduce astigmatism in a resonator, i.e. the focus positions in the tangential and sagittal planes are different. By a proper choice of the AOI

#188266 - $15.00 USD Received 3 Apr 2013; revised 23 Apr 2013; accepted 27 Apr 2013; published 3 May 2013

the astigmatism can be turned into a pure ellipticity. In particular, this is the case for identical focusing mirrors with equal angles of incidence. Close to the stability edges, the ellipticity diverges, i.e. the illuminated area is not as large as for a round beam.

Thus, it is highly desirable to compensate for the ellipticity. In lasers, Brewster cells (e.g. the laser crystal) are usually employed for astigmatic compensation [36]. However, for high-power ECs, any transmissive element introduces detrimental effects, such as damage, polarization discrimination, dispersion and nonlinearities. However, the ellipticity can be compensated by introducing a slight additional curvature to the surfaces of the cavity optics, i.e. with purely reflective optics. Here, we propose three ways of astigmatic compensation for the SBT design sketched in Fig. 1(a):

- Replacing two plane mirrors by two identical cylindrical mirrors with a weak curvature (either convex in the tangential plane, or concave in the sagittal plane).
- Replacing the two spherical mirrors by two identical toroidal mirrors with a weak curvature difference in the two planes.
- Both methods may be implemented by elastic deformation of the plane or curved mirrors, respectively.

Using this scheme with the SBT at the inner stability edge, an eigenmode that is large and round on all optics may be obtained. As symmetry with respect to the focal planes is preserved, the focal positions are equal in the tangential and sagittal plane and there is no ellipticity. In the following, we denote such an astigmatism-free SBT cavity close to the inner stability edge "Large-Mode-Bow-Tie" (LMBT).

In Fig. 5(a), the beam radii of an SBT with 600 mm radius of curvature are shown with and without astigmatic compensation. In this example, the two plane mirrors are replaced by two cylindrical mirrors defocusing in the tangential plane with radius of curvature of -100 m. For an AOI of 4.4°, the ellipticity is totally removed. Here the AOI was increased artificially, which allows for the use of readily available cylindrical mirrors. Figure 5(b) shows the ellipticity (calculated in the focus) as a function of Δ (as shown in Fig. 1) for different spot sizes. For larger spot sizes a better alignment accuracy is required. With weaker cylindrical mirrors, the compensation is achieved for smaller AOI, requiring less accuracy. Note that the compensation does not change the type of the stability edge, i.e. the alignment sensitivity can be read off Fig. 2.2 from the lower branch of the SBT. The only additional constraint is the alignment of Δ as shown in Fig. 5(b). This all-reflective compensation scheme allows for a round beam on all cavity optics even at the stability edge with commercially available mirrors and realistic requirements on the alignment accuracy.

5.2. Non-planar cavities

In a non-planar cavity configuration, the transverse ellipticity of the eigenmode can be removed by a proper choice of the angles of incidence on the spherical mirrors. Without the constraint that the beam must propagate in a single plane during the entire roundtrip, axial symmetry can be achieved rendering additional curved elements for ellipticity compensation unnecessary. For a non-planar EC, however, the polarization of the circulating light depends on that of the incoming light, on the geometric rotation due to the non-planar propagation and on the resonator finesse [37, 38]. While this feature could in principle be used for various applications, both the theoretical description and the experimental handling of a non-planar cavity are more involved than those of a planar cavity due to the lack of well-defined tangential and sagittal planes. The non-planar case exceeds the scope of this paper and will be treated in a future publication.

#188266 - $15.00 USD Received 3 Apr 2013; revised 23 Apr 2013; accepted 27 Apr 2013; published 3 May 2013

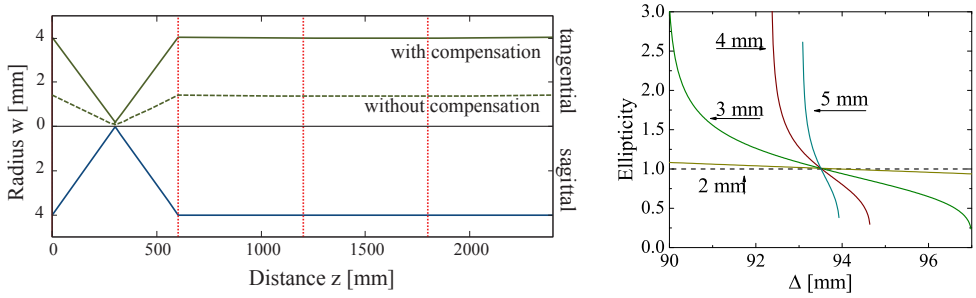

(a) (b)

Fig. 5. (a) Beam radius of a 125 MHz SBT cavity as described in the text with and without astigmatic compensation. The dotted red lines indicate the positions of the mirrors.
(b) Beam ellipticity w_x/w_y at the mirrors as a function of the distance Δ as defined in Fig. 1 for different spot sizes.

6. Conclusion

A major limitation of power scaling of ultrashort pulses in state-of-the-art enhancement cavities (ECs) is mirror damage induced by intensity-related and/or thermal effects [4]. Here, we addressed the design of robust ECs with large spot sizes on all optics, a measure that promises to mitigate this limitation by decreasing both the intensity and the thermal gradient on the optics' surfaces. To quantify the sensitivity of ECs towards perturbations we evaluate the overlap between the cavity eigenmodes before and after a perturbation. This metric enables the comparison of various cavity designs. In particular, it identifies the standard bow-tie (SBT) ring resonator consisting of two spherical mirrors and several additional folding mirrors, operated close to the inner stability edge, as the most robust approach to large-mode ECs. We investigated two large-mode cavity designs experimentally: the above-mentioned SBT and an all-curved-mirror (ACM) resonator consisting of 4 identical spherical mirrors, both with a repetition rate of 125 MHz. The misalignment sensitivity predicted by the overlap metric is confirmed qualitatively by the behavior of the two resonators: while the ACM cavity can hardly be aligned with standard mechanics for beam radii larger than 4 mm, the SBT configuration readily allows for beam radii of 5.7 mm (only limited by the mirror size) without a considerably increased alignment difficulty compared to the center of the stability range. In our experiment, the illuminated area on all mirrors was increased by a factor of 15 compared to the system described in [4]. At the same position in the stability range, an additional factor of about 2 in area as well as a round mode shape throughout the resonator would be obtained by compensating for the strong ellipticity using cylindrical or toroidal mirrors. The design strategies and tools developed here are expected to have a significant impact on the scaling of the attainable power and peak intensity levels in ECs driven by ultrashort pulses and their applications.

Acknowledgments

This work was supported by the Deutsche Forschungsgemeinschaft (DFG) Cluster of Excellence, Munich Centre for Advanced Photonics (MAP) (www.munich-photonics.de), by the KORONA Max-Planck-Institut für Quantenoptik (MPQ)/Fraunhofer Institut für Lasertechnik (ILT) cooperation and by the Bundesministerium für Bildung und Forschung (BMBF) under PhoNa - Photonische Nanomaterialien, contract number 03IS2101B.

#188266 - $15.00 USD Received 3 Apr 2013; revised 23 Apr 2013; accepted 27 Apr 2013; published 3 May 2013